8

Cerenkov counters

The Cerenkov (or Cherenkov) effect occurs when the velocity of a charged particle traversing a dielectric medium exceeds the velocity of light in that medium. A small number of photons will be emitted at a fixed angle, which is determined by the velocity of the particle and the index of refraction of the medium. The light may then be collected onto a photomultiplier tube to form a counter. A threshold Cerenkov counter detects the presence of a particle whose velocity exceeds some minimum amount, while a differential Cerenkov counter can measure the velocity of a particle within a certain range. Lead-glass Cerenkov counters are widely used for the detection of photons.

8.1 The Cerenkov effect

Early investigations of radioactivity had observed that radioactive substances produced a pale light when placed in certain liquids. The effect is named after the Russian physicist Cerenkov, who conducted a thorough investigation of the phenomenon in the 1930s. The Cerenkov effect occurs when the velocity of a charged particle exceeds the velocity of light in a dielectric medium (c/n), where n is the index of refraction for the medium [1, 2]. Excited atoms in the vicinity of the particle become polarized and coherently emit radiation at a characteristic angle θ, determined from the relation

$$\cos \theta = 1/\beta n \tag{8.1}$$

with $\beta > 1/n$.

The index of refraction of materials is a function of wavelength and temperature. Figure 8.1 shows the variation of n with wavelength for several materials. There is a general tendency for n to decrease with

https://doi.org/10.1017/9781009290098.009 Published online by Cambridge University Press

increasing λ. The variation $dn/d\lambda$ is referred to as dispersion. The dispersion is largest in the ultraviolet (*uv*) portion of the spectrum. The variation with temperature is generally small, for example, $dn/dT \simeq -15 \times 10^{-6}/°C$ for BaF_2 in the visible spectrum.

Values of $\cos\theta$ as a function of the particle's velocity β are shown in Fig. 8.2 for various values of n. Note that according to Eq. 8.1 there is a threshold velocity $\beta_t = 1/n$ below which no light is emitted. As the particle velocity increases beyond β_t, the light is given off at larger and larger angles up to a maximum $\theta_{max} = \cos^{-1}(1/n)$ which occurs for $\beta = 1$.

The threshold relation given above is strictly only true for an infinite radiator medium. In this case the angular distribution of emitted radiation is a delta function at the angle θ. For finite radiation lengths a more complete treatment shows that the angular distribution contains secondary minima and maxima [3]. However, in this discussion we will ignore any fine structure in the Cerenkov spectrum.

The Huyghen's construction derivation of Eq. 8.1 is shown in Fig. 8.3. The positions of the particle and expanding spheres of radiation are shown for four instances of time. The tangent planes to the spheres represent a plane electromagnetic wave propagating through the medium at an

Figure 8.1 Index of refraction of various materials as a function of wavelength. The vertical dashed line is the location of the sodium *D* line, which is often used for quoting *n* values. (Data from *American Institute of Physics Handbook,* 3rd ed., New York: McGraw-Hill, 1972.)

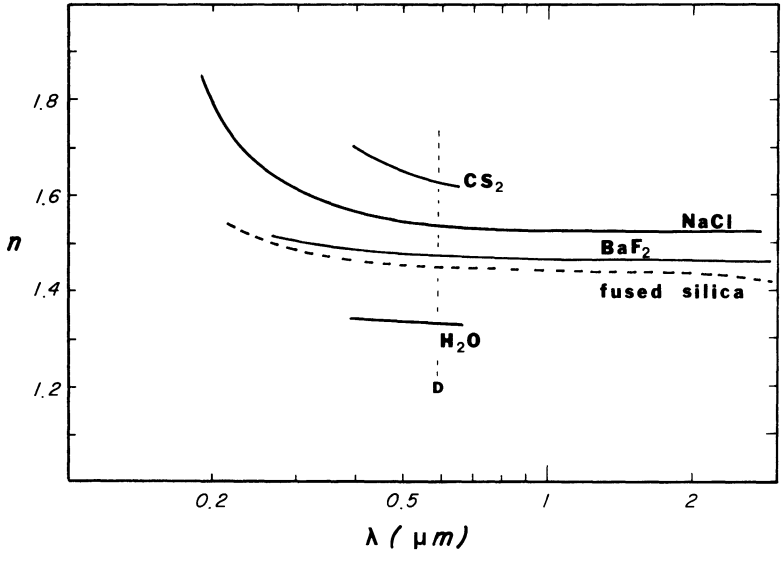

https://doi.org/10.1017/9781009290098.009 Published online by Cambridge University Press

angle θ with respect to the particle's trajectory. It can be seen that a coherent wavefront can be constructed when $\beta > \beta_t$ but not when $\beta < \beta_t$.

An explanation of the effect using classical electrodynamics was given in 1937 by Frank and Tamm [1, 2]. They considered an electron moving with constant velocity through a perfect, isotropic dielectric. All the properties of the medium were encompassed in the dielectric constant or, equivalently, in the index of refraction. The solution of Maxwell's equations for the case $\beta n > 1$ has the form of a traveling electromagnetic wave.

The amount of energy emitted per unit length and per unit frequency interval $d\omega$ by a particle with charge Ze is given by

$$\frac{dE}{dx\, d\omega} = \frac{Z^2 r_e mc^2}{c^2}\left(1 - \frac{1}{\beta^2 n^2}\right)\omega \tag{8.2}$$

where r_e is the classical radius of the electron. Note that the emitted radiation increases linearly with the frequency ω and with the square of the particle's charge. For the following discussion we consider singly charged particles. It is usually more convenient to express Eq. 8.2 in terms of the wavelength λ of the radiation

$$\frac{dE}{dx\, d\lambda} = 4\pi^2 r_e mc^2 \frac{1}{\lambda^3}\left(1 - \frac{1}{\beta^2 n^2}\right) \tag{8.3}$$

Figure 8.2 Cerenkov angle θ versus particle velocity β for various values of the refractive index n.

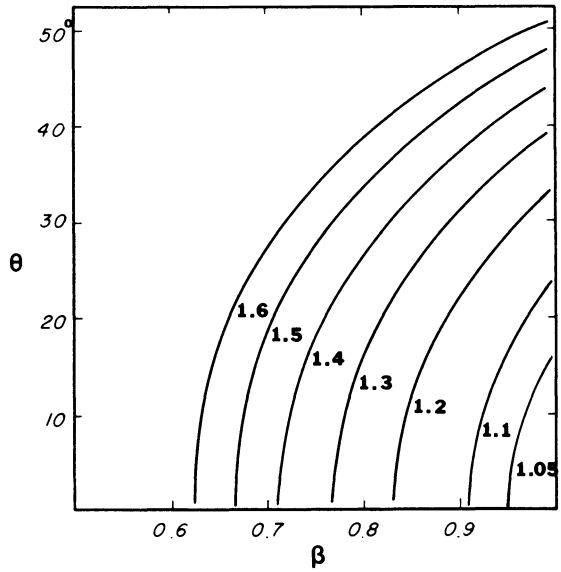

https://doi.org/10.1017/9781009290098.009 Published online by Cambridge University Press

The emitted energy is strongly peaked at short wavelengths. We can rewrite Eq. 8.3 in terms of the number N of emitted photons as

$$\frac{dN}{dx\,d\lambda} = 2\pi\alpha\frac{1}{\lambda^2}\left(1 - \frac{1}{\beta^2 n^2}\right) \tag{8.4}$$

where α is the fine structure constant. The total number of photons emitted per unit path length is

$$\frac{dN}{dx} = 2\pi\alpha \int_{\beta n > 1} \left(1 - \frac{1}{\beta^2 n^2(\lambda)}\right)\frac{d\lambda}{\lambda^2} \tag{8.5}$$

Figure 8.3 Huyghen's construction of the expanding spherical wavefronts at three instances of time.

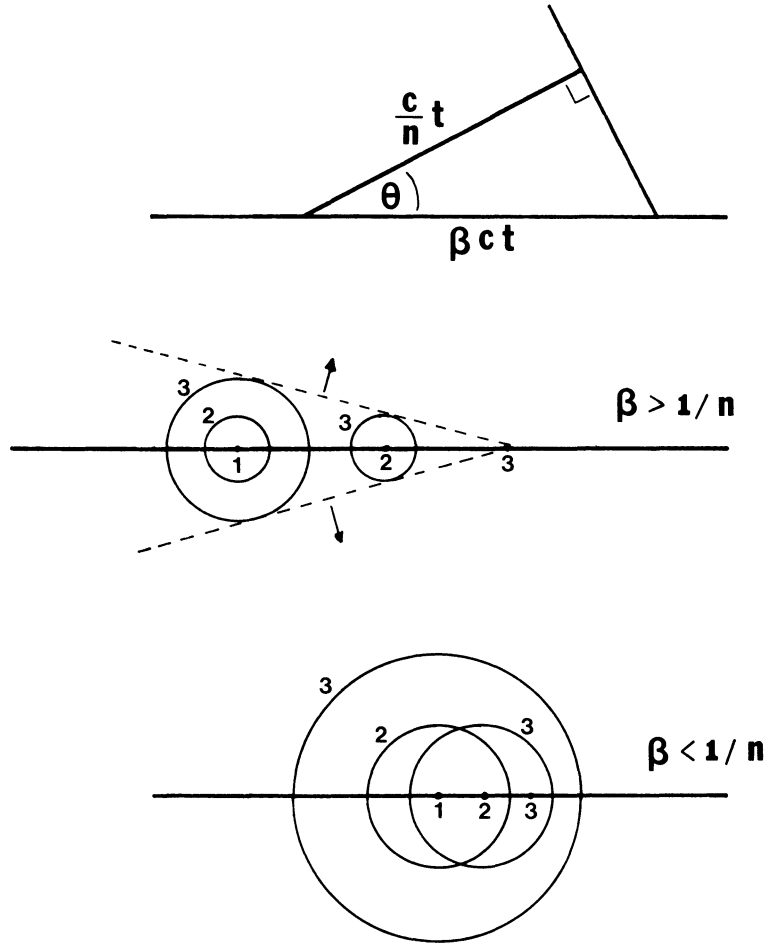

https://doi.org/10.1017/9781009290098.009 Published online by Cambridge University Press

In practice, the condition $\beta n > 1$ is only satisfied for the ultraviolet to near infrared portion of the electromagnetic spectrum.

If the variation in $n(\lambda)$ is small over the wavelength region λ_1 to λ_2, the energy emitted per unit length becomes

$$\frac{dE}{dx} = 2\pi^2 r_e mc^2 \sin^2\theta \left(\frac{1}{\lambda_1^2} - \frac{1}{\lambda_2^2}\right) \tag{8.6}$$

while the photon yield is

$$\frac{dN}{dx} = 2\pi\alpha \sin^2\theta \left(\frac{1}{\lambda_1} - \frac{1}{\lambda_2}\right) \tag{8.7}$$

For example, using the wavelength interval 350–500 nm, corresponding roughly to the response range of photomultiplier tubes with Sb–Cs pho-

Table 8.1. *Properties of liquid and solid radiators*

Material	Formula	n^a	ρ (g/cm^3)
FC-75	$C_8F_{16}O$	1.276	1.76
Water	H_2O	1.333	1.00
1-Butanol	C_4H_9OH	1.397	0.810
Carbon tetrachloride	CCl_4	1.459	1.591
Glycerol	$C_3H_5(OH)_3$	1.474	1.26
Toluene	$C_6H_5CH_3$	1.494	0.867
Styrene	$C_6H_5CHCH_2$	1.545	0.910
Carbon disulfide	CS_2	1.628	1.263
Diiodomethane	CH_2I_2	1.749	3.325
Lucite	$C_5H_8O_2$	1.49	1.16–1.20
Plastic scintillator	—	1.58	1.03
Pilot 425	—	1.49	1.19
Crystal quartz	SiO_2	1.54	2.65
Borosilicate glass		1.474	2.23
Lithium fluoride	LiF	1.392	2.635
Barium fluoride	BaF_2	1.474	4.89
Sodium iodide	NaI	1.775	3.667
Cesium iodide	CsI	1.788	4.51
Bismuth germanate	$Bi_4Ge_3O_{12}$	2.15	7.13
Sodium chloride	NaCl	1.544	2.165
Silica aerogel	$n(SiO_2) + 2n(H_2O)$	$1 + 0.25\rho$	0.1–0.3

[a] For sodium light at 20–25°C.

Source: Handbook of Chemistry and Physics, 64th ed., Boca Raton: CRC Press, 1983; Particle Data Group, Rev. Mod. Phys. 56: S1, 1984; *American Institute of Physics Handbook,* 3rd ed., New York: McGraw-Hill, 1972; Catalog, Nuclear Enterprises.

tocathodes deposited on glass, we find

$$dE/dx = 1180 \sin^2\theta \quad \text{eV/cm}$$
$$dN/dx = 390 \sin^2\theta \quad \text{photons/cm} \tag{8.8}$$

Indices of refraction of some common liquids and solids are given in Table 8.1. For a singly charged particle with $\beta \sim 1$ traversing water ($n = 1.33$), the Cerenkov angle is 41.2°. This implies that 513 eV/cm is given off as Cerenkov radiation. Note that this is small compared to the ~ 2 MeV/cm ionization energy loss and 100 times weaker than the light output in plastic scintillator. On the average, 170 photons will be emitted per centimeter of path length. Examining Table 8.1, note that FC-75 is a fluorocarbon with the lowest index of refraction for a room temperature liquid.

The Cerenkov light is emitted almost instantaneously. The angular distribution of the light intensity is approximately a δ function at the Cerenkov angle. The actual distribution is broadened due to dispersion, energy loss of the particle, multiple scattering, and diffraction.

8.2 Photon yield

We have seen that an important aspect of Cerenkov radiation is the small light yield compared to a scintillation counter of comparable thickness. The small photon yield means that the pulses from the counter are small with large fluctuations. Thus, every effort must be made to collect as many photons as possible. Since the bulk of the deposited Cerenkov energy is in the ultraviolet portion of the spectrum, special steps can be taken to see that these photons are accepted. If we want to ensure that fluctuations in the number of photoelectrons emitted from the photomultiplier do not play a significant role in determining the efficiency of the counter, then the counter should be designed so that at least 20 photoelectrons are emitted per particle.

Typical threshold and differential counters are shown in Fig. 8.4. The Cerenkov radiator should be transparent to the emitted radiation over the desired wavelength range. The radiator should not produce scintillation light. It is desirable to have a large index of refraction since the intensity $I \propto 1 - (\beta n)^{-2}$. In addition, the radiator should have small density and atomic number in order to minimize ionization loss and multiple scattering. The refractive indices of the radiator, optical grease, and PMT window should be as identical as possible. For example, for $n_{\text{rad}} = 1.6$ and $n_{\text{grease}} = 1.4$, a particle with $\beta \sim 1$ and incident at an angle $>30°$ to the photocathode plane, over 50% of the light is reflected [2].

https://doi.org/10.1017/9781009290098.009 Published online by Cambridge University Press

Figure 8.4 Construction of typical threshold and differential Cerenkov counters. (PM) photomultiplier tube, (M) mirror, (P) particle moving along the counter axis, and (d) slit diaphragm. (J. Litt and R. Meunier, adapted with permission from the Annual Review of Nuclear Science, Vol. 23, © 1973 by Annual Reviews Inc.)

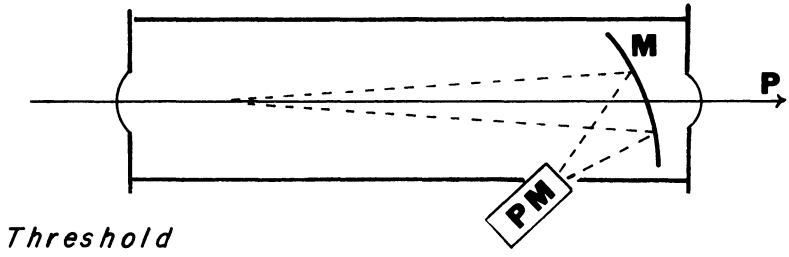

Threshold

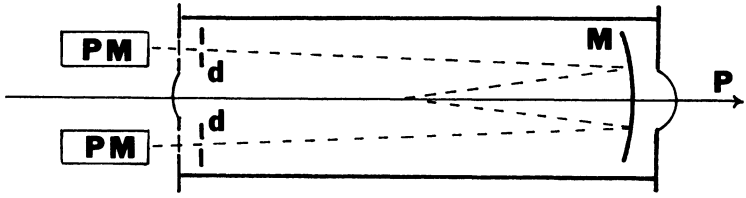

Differential

Figure 8.5 The reflectance at normal incidence from metallic surfaces. (Data from *Handbook of Chemistry and Physics,* 64th ed., Boca Raton: CRC Press, 1983.)

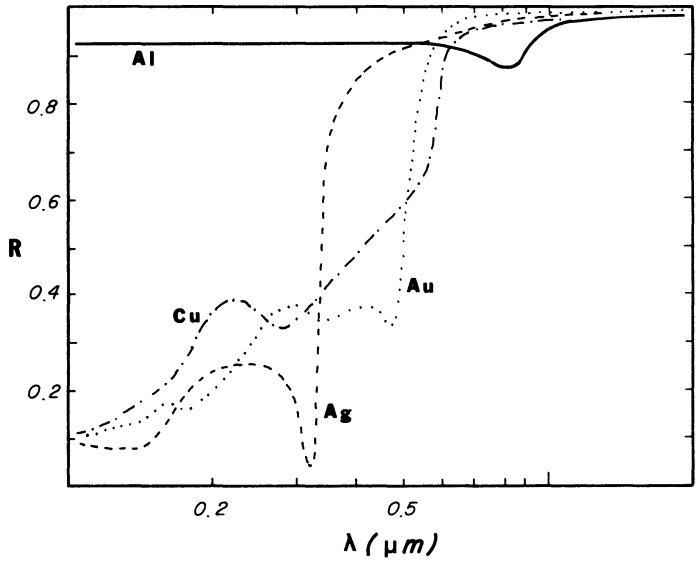

https://doi.org/10.1017/9781009290098.009 Published online by Cambridge University Press

The light collection system should be as efficient as possible. This requirement is aided by the directionality exhibited by Cerenkov radiation. Simple optical arrangements can be used to gather the produced light and focus it onto the face of the PMT. The optics should be designed to minimize the light lost in reflections. The reflection coefficient for light at normal incidence on metallic surfaces is shown in Fig. 8.5. In the visible spectrum an evaporated gold layer has high reflectance. However, in the near ultraviolet region aluminum has a much higher reflectance. White paper or layers of MgO also have good reflectance in the visible. Thin layers of MgF_2 can be applied to surfaces to alter the ultraviolet reflection properties [4].

Another important consideration is transmission of the light through any windows in the optical system [5]. Transparent materials generally have absorption bands in the infrared and ultraviolet portions of the spectrum. Table 8.2 lists the regions over which various materials have a

Table 8.2. *Transmittance regions of various materials*[a]

Material	Lower limit (μm)	Upper limit (μm)
Magnesium fluoride	0.11	7.5
Lithium fluoride	0.12	9.0
Calcium fluoride	0.13	12
Sodium fluoride	0.19	15
Sodium chloride	0.21	26
Potassium chloride	0.21	30
Silver chloride	0.4	28
Potassium bromide	0.25	40
Potassium iodide	0.25	45
Cesium iodide	0.25	80
Magnesium oxide	0.25	8.5
Crystal quartz	0.12	4.5
Fused silica	0.12	4.5
Borosilicate glass	0.4	3.5
Sapphire	0.14	6.5
Diamond	0.25	80
Gallium arsenide	1.0	15
Silicon	1.2	15
Germanium	1.8	23

[a] Region between limits of 10% external transmittance for 2-mm-thick samples.
Source: American Institute of Physics Handbook, 3rd ed., New York: McGraw-Hill, 1972.

transmission greater than 10%. For efficient detection of ultraviolet light it is obviously important that the lower transmission limit be as small as possible. Ordinary borosilicate glass only transmits down to ~300 nm. Quartz, fused silica, and MgF_2 crystals can be used as window materials to maximize the acceptance of ultraviolet light.

High quality PMTs are necessary for single particle detection. It may be necessary to work with electronic thresholds below the single photoelectron level. The tube should have a high quantum efficiency, low dark current, good signal to noise, and no afterpulsing. The output of the tube can be used in a coincidence arrangement to minimize accidental counting. The window of the tube should have good ultraviolet transmission. A PMT window made of quartz or fused silica can extend the light transmission below 200 nm. An antireflection layer of MgF_2 can be deposited on the window. Special photocathode materials can also help extend the photomultiplier acceptance into the ultraviolet.

The photoelectron output of a given PMT is obtained by convoluting the frequency spectrum of produced Cerenkov radiation with the frequency response of the collection system and tube. Thus, using Eq. 8.4 for the number of photons produced per unit path, we find that the number of emitted photoelectrons in the tube per unit particle pathlength is

$$dN_e/dx = 2\pi\alpha \int \left(1 - \frac{1}{\beta^2 n^2}\right) \epsilon_c(\lambda) \frac{S(\lambda)}{\lambda^2} d\lambda \tag{8.9}$$

where $\epsilon_c(\lambda)$ is the efficiency for collecting photons of wavelength λ at the cathode and $S(\lambda)$ is the normalized relative response of the photomultiplier. The number of photoelectrons is frequently written in the form

$$N_e = N_0 L \sin^2\theta \tag{8.10}$$

where L is the length of the radiator and the various efficiencies and spectral responses are incorporated in the constant N_0.

An alternative method of enhancing the photon yield is to use a wavelength shifter to shift the ultraviolet region of the production spectrum to the visible region, where ordinary PMTs are most sensitive. A small concentration of photoluminescent atoms can be added to the radiator, window, or PMT face. The shifter tends to make the radiation more isotropic, and hence the collimation properties of the Cerenkov light are lost when the shifter is added to the radiator. However, this is not a problem when the shifter is applied to the PMT window [2].

8.3 Gas radiators

Cerenkov counters using a gas radiator are particularly useful for detecting particles with $\beta > 0.99$. The refractive indices of gases in the

visible and ultraviolet depend critically on the presence of absorption bands. The index of refraction of the gas is related to its density ρ through the Lorenz–Lorentz law [2]

$$\frac{n^2-1}{n^2+2}\frac{M}{\rho}=R \tag{8.11}$$

where M is the molecular weight and R is the molecular refraction coefficient. The constant R approximately equals the volume occupied by 1 mol of the gas excluding empty space.

Since for gases $n \simeq 1$, we can rewrite Eq. 8.11 to a high degree of accuracy as

$$n-1 \simeq \frac{3}{2}\frac{R}{M}\rho \tag{8.12}$$

From the ideal gas law we have

$$P=\rho R'T/M \tag{8.13}$$

where P is the pressure, T is the absolute temperature, and R' the gas constant. Substituting into Eq. 8.12, we obtain

$$n-1=(n_0-1)P/P_0 \tag{8.14}$$

where the subscript 0 indicates that the quantity is measured at atmospheric pressure. Using the notation $\eta = n-1$, we can express this as

$$\eta=\eta_0 P/P_0 \tag{8.15}$$

The indices of refraction of a number of gases are listed for atmospheric pressure in Table 8.3. Also listed are the critical temperature and critical pressures of the gases. The critical temperature is the temperature above which a gas cannot be liquified using pressure alone. The critical pressure is the pressure at which gas and liquid exist in equilibrium when at the critical temperature.

The threshold of a gas counter can be adjusted by varying the pressure. The following relations are useful in understanding the properties of gas counters as a function of momentum ($=m\beta\gamma$).

$$\sin^2\theta=\beta_t^2\left(\frac{1}{\beta_t^2\gamma_t^2}-\frac{1}{\beta^2\gamma^2}\right) \tag{8.16}$$

$$\begin{aligned}\beta_t\gamma_t &= \frac{1}{\sqrt{n^2-1}} \\ &\simeq \frac{1}{\sqrt{2\eta}}\end{aligned} \tag{8.17}$$

Using Eq. 8.15, we find that

https://doi.org/10.1017/9781009290098.009 Published online by Cambridge University Press

Table 8.3. *Properties of gas radiators, STP*

Gas	Formula	η_0[a] ($\times 10^{-4}$)	θ_{max} (degrees)
Helium	He	0.35	0.48
Neon	Ne	0.67	0.66
Hydrogen	H_2	1.38	0.95
Oxygen	O_2	2.72	1.33
Argon	Ar	2.84	1.36
Nitrogen	N_2	2.97	1.40
Methane	CH_4	4.41	1.70
Carbon dioxide	CO_2	4.50	1.72
Ethylene	C_2H_4	6.96	2.14
Ethane	C_2H_6	7.06	2.15
Freon 13	$CClF_3$	7.82	2.27
Sulfur hexafluoride	SF_6	7.83	2.27
Propane	C_3H_8	10.05	2.57
Freon 12	CCl_2F_2	11.27	2.72
Freon 114	$C_2Cl_2F_4$	14	3.03
Pentane	C_5H_{12}	17.1	3.3

[a] At 589 nm.

Source: J. Jelley, *Cerenkov Radiation and its Applications,* London: Per
tion in High Energy Physics, Federal Scientific and Technical Informa
Cerenkov Counters, in High Energy and Nuclear Physics Data Book,

$$\beta_t\gamma_t \simeq \left(\sqrt{2\eta_0 \frac{P}{P_0}}\right)^{-1} \tag{8.18}$$

We see that increasing the pressure brings the momentum threshold down like $1/\sqrt{P}$. The threshold dependence of several gases determined from Eq. 8.18 is shown in Fig. 8.6.

For a beam of fixed velocity particles the intensity of the Cerenkov radiation varies with pressure like

$$\sin^2\theta = 1 - \frac{1}{\beta^2(1 + kP)^2} \tag{8.19}$$

Figure 8.6 Thresholds for gases versus absolute pressure.

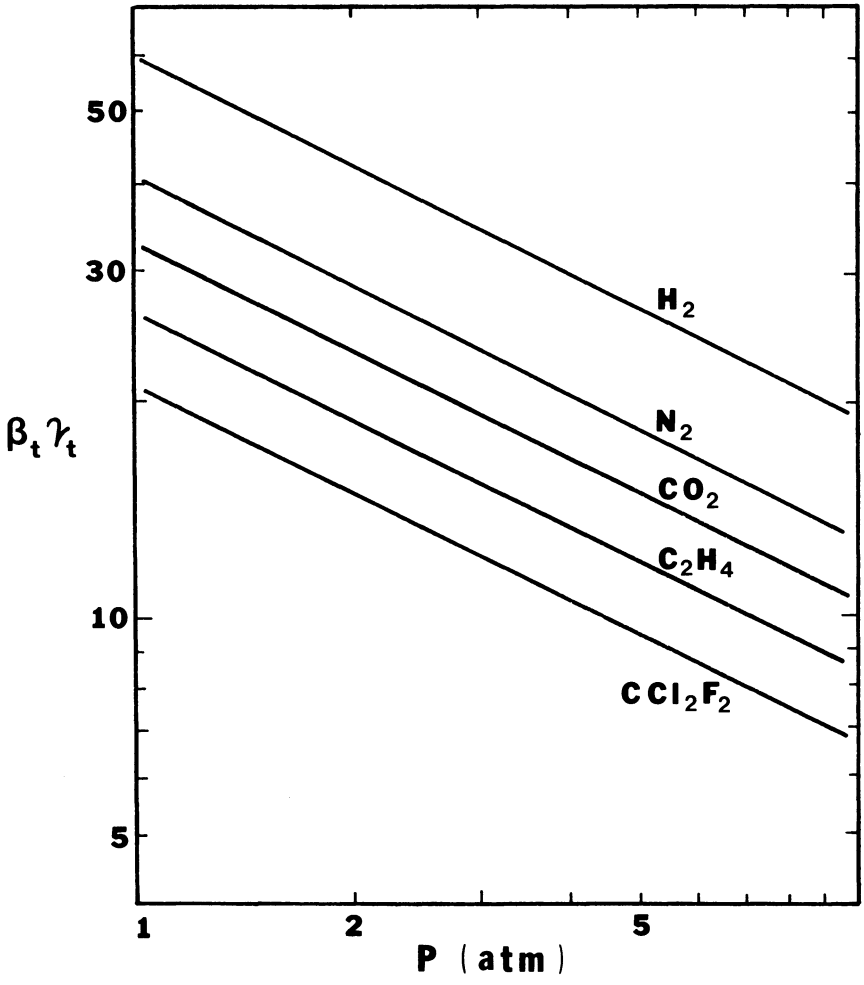

https://doi.org/10.1017/9781009290098.009 Published online by Cambridge University Press

where

$$k = (n_0 - 1)/P_0 \tag{8.20}$$

The intensity is 0 until the pressure satisfies $\beta n = 1$. Then, following a threshold knee, we have ($\beta \approx 1$)

$$\sin^2\theta \simeq 2kP \tag{8.21}$$

and thus the intensity goes up linearly with pressure.

A simple pressure manometer is usually not sufficiently accurate for determining the index of refraction [2]. The pressure may be determined to greater precision using a pressure sensitive capacitance transducer, or the index of the gas may be measured directly using an interferometer.

A simple interferometer may be constructed by connecting a gas line from the counter to a small chamber containing accurately positioned Fabry–Perot plates. Light from a laser will undergo multiple reflections between the plates. A photodiode located at a fixed angle on the opposite side of the chamber from the laser can be used to measure the relative amount of transmitted light. If the gas in the chamber is slowly evacuated, the conditions for constructive interference change, resulting in a series of light and dark fringes appearing at the photodiode. The number of such fringes can be simply related to the absolute value of the refractive index.

8.4 Threshold counters

We have seen that no Cerenkov radiation is produced until the velocity of the particle exceeds a minimum value $\beta_t = 1/n$. Because of this, a Cerenkov counter can be used as a threshold device to indicate the presence of a particle whose velocity exceeds a certain minimum value. Sets of counters are commonly used this way to identify particles with different masses in a beam of fixed momentum.

Gas counters are particularly advantageous for high momentum particles since indices of refraction near 1 are required, and the indices of gases near this value can be controlled by varying the pressure of the gas. A simple threshold counter was shown in Fig. 8.4. The radiator gas is contained in a high pressure, light tight container. Cerenkov light is reflected by the mirror and transmitted through a pressure window onto the PMT. As the pressure is raised, thresholds for various mass particles are passed, and the counting rate passes through plateaus. The levels of the plateaus allow a determination of the relative particle abundances in a beam.

A class of Cerenkov counters uses total internal reflection as a filter for the collection of light [1, 2]. Consider a particle traversing normally a wide, relatively thin slab of material bounded on the exit side by air. The

Cerenkov light in the material will pass through the exit face provided that the Cerenkov angle is smaller than the critical angle. Thus, the detected particles satisfy the relation

$$\cos^{-1}(1/n\beta) \leqslant \sin^{-1}(1/n) \tag{8.22}$$

The counter detects particles over a velocity range starting at $\beta_t = 1/n$ and continuing up to

$$\beta_{max} = (n^2 - 1)^{-1/2} \tag{8.23}$$

instead of $\beta_{max} = 1$. Total internal reflecting counters have been constructed using lucite as a radiator.

The detection efficiency of a threshold counter increases rapidly as the velocity of the incident particles increases over the calculated threshold velocity. The detection efficiency can be found experimentally with the counter arrangement in Fig. 8.7. The Cerenkov counter efficiency is given by the ratio of coincidences $S_1 \cdot S_2 \cdot C/S_1 \cdot S_2$.

The detection efficiency may be calculated as

$$\epsilon(\beta) = 1 - \Pr(0, N_e) \tag{8.24}$$

where $\Pr(0, N_e)$ is the probability that no electrons were emitted by the photocathode of the PMT if the average number is N_e. According to Eq. 8.9, N_e depends on β, the collection efficiency, and the quantum efficiency of the tube. Since the photoelectron emission follows a Poisson distribution, we have

$$\epsilon(\beta) = 1 - \exp(-N_e) \tag{8.25}$$

Since $\Pr(0, 5) = 0.01$, we must have an average of five emitted electrons to achieve a 99% detection efficiency. The efficiency curve rises more quickly if the radiator length L or quality factor N_0 is increased, since more photons would be available on the average. In addition, the shape of the efficiency curve is affected by energy loss in the gas, dispersion, and the velocity spread of the incident beam [2].

The threshold velocity resolution of the counter can be determined

Figure 8.7 A simple arrangement for measuring Cerenkov counter efficiencies. S_1 and S_2 are scintillation counters, C is the Cerenkov counter.

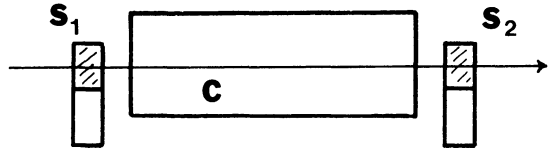

https://doi.org/10.1017/9781009290098.009 Published online by Cambridge University Press

from Eq. 8.10, which we rewrite in the form

$$N_e(\beta) = N_0 L(1 - \beta_t^2/\beta^2) \tag{8.26}$$

Only keeping terms to first order in the quantity $\Delta\beta = \beta - \beta_t$, we find that

$$\frac{\Delta\beta}{\beta_t} = \frac{N_e}{2(N_0 L - N_e)} \tag{8.27}$$

It is desirable that a threshold counter achieve near 100% efficiency as quickly as possible after the particle velocity increases over threshold. For any required number of photoelectrons, the threshold velocity resolution will be improved by designing the quantity $N_0 L$ to be as large as possible.

In order to calculate the efficiency as a function of momentum, we can use Eq. 8.16 to write the mean number of photoelectrons as

$$N_e = N_0 L\beta_t^2 \left(\frac{1}{\beta_t^2\gamma_t^2} - \frac{1}{\beta^2\gamma^2}\right) \tag{8.28}$$

For a particle of mass m

$$N_e(p) = N_0 L\beta_t^2 m^2(1/p_t^2 - 1/p^2) \tag{8.29}$$

where p_t is the threshold momentum. The efficiency can be found by substituting $N_e(p)$ into Eq. 8.25.

The behavior of the detection efficiency near threshold can be affected by the production of knock on electrons (delta rays). It is possible for a massive particle with $\beta < \beta_t$ to collide with an electron and knock it out with velocity greater than β_t. The number of photons $N(E)$ in the wavelength interval λ_1 to λ_2 emitted by a delta ray with initial kinetic energy E is given by [2]

$$N(E) = 2\pi\alpha \int_{\lambda_1}^{\lambda_2} \frac{d\lambda}{\lambda^2} \int_{E_t}^{E_{max}} \left(1 - \frac{(E + mc^2)^2}{n^2(E + 2mc^2)E}\right) dE \frac{dx}{dE} \tag{8.30}$$

where m is the mass of the electron, E_t is the threshold energy for Cerenkov radiation, and E_{max} is the maximum energy of the delta rays. The threshold energy depends on n through the relation

$$E_t = \frac{mc^2}{\sqrt{1 - 1/n^2}} \tag{8.31}$$

while the maximum energy of a delta ray is given by Eq. 1.24, $E_{max} = 2mc^2\beta^2\gamma^2$. Thus, the maximum electron energy increases for increasing β and equals 9.5 MeV for an incident particle with $\beta = 0.95$. Fortunately, the delta rays are emitted with an angular distribution [2]

$$\frac{dN}{d\theta} \simeq \frac{\sin\theta}{\cos^3\theta} \tag{8.32}$$

https://doi.org/10.1017/9781009290098.009 Published online by Cambridge University Press

so that almost all of them come off perpendicularly to the direction of the heavy incident particle.

In gas threshold counters the choice of gas and operating pressure are determined by the desired value of γ_t. The amount of dispersion and multiple scattering may also have to be considered. The diameter of the counter must be matched to the maximum angle of radiation emission, while the length is determined by the required photon yield. Some properties of gas threshold counters currently in use are shown in Table 8.4.

Now let us consider some examples of threshold counters [6]. The TASSO group at DESY has incorporated gas and silica aerogel threshold counters into their particle spectrometer [7]. Silica aerogel consists of strings of small (~4-nm-diameter) spheres of amorphous silica surrounding spheres (~60-nm diameter) of trapped air [8]. The index of refraction of the solid material can be lowered from the value for pure silica ($n = 1.46$) by increasing the amount of trapped air. It is possible by this means to obtain a transparent solid material with a small value of n. The TASSO aerogel blocks were constructed with $n = 1.024$.

Table 8.4. *Examples of Cerenkov counter systems*

Detector	Location	Type	Medium	Pressure (atm)	Photon detection
AFS	ISR	threshold	Freon 12	4	
DELCO	PEP	threshold	isobutane	1	RCA8854
EMC	SPS	threshold	Ne, N_2	1	XP2041
Exp. 605	FNAL	RICH	He	1	PWC
HRS	PEP	ultraviolet	Ar-N_2	15	PWC
IMB	Ohio	p decay	water	1	EMI9870B
Kamiokande	Japan	p decay	water	1	R1449X
LASS	SLAC	threshold	Freon 114	1	
MD1	Novosibirsk	threshold	ethylene	25	
MPS II	BNL	threshold	Freon 12	3	RCA4501
Tagged γ	FNAL	threshold	N_2	1	
TASSO	PETRA	threshold	aerogel	1	RCA8854
		threshold	Freon 114	1	XP2041
		threshold	CO_2	1	XP2041

Source: Particle Data Group, Major detectors in elementary particle physics, Report LBL-91, UC-37, 1983; H. Gordon et al., Nuc. Instr. Meth. 196: 303, 1982; W. Slater et al., Nuc. Instr. Meth. 154: 223, 1978; Y. Declais et al., Nuc. Instr. Meth. 180: 53, 1981; G. Coutrakon et al., IEEE NS-29: 323, 1982; J. Chapman, N. Harnew, and D. Meyer, IEEE NS-29: 332, 1982; H. Burkhardt et al., Nuc. Instr. Meth. 184: 319, 1981.

The gas counters shown in Fig. 8.8 use CO_2 and Freon 114 radiators at atmospheric pressure. Concave ellipsoidal mirrors were used with one focus at the e^+e^- interaction point and the other at the PMT. The mirrors were formed from heat-treated lucite sheets with a vacuum-deposited aluminum surface. The reflectivity was around 90%. Winston cones were used to collect the light. The cathode of the XP2041 PMT was coated with wavelength shifter to improve the ultraviolet response. The efficiency of the Freon 114 counter is shown in Fig. 8.9 as a function of the pion momentum.

One difficulty with collecting the light from the aerogel counter is that visible light has a high probability for scattering. The measured scattering length is 2.4 cm at a wavelength of 436 nm [7]. In this case a light collection system using diffuse scatterings was more efficient than one using focusing mirrors. Figure 8.10 shows a plateau above 1 GeV/c in the aerogel efficiency as a function of pion momentum. The mean number of photoelectrons in the plateau is shown as a function of aerogel thickness in Fig. 8.10b. The number differs from the linear dependence predicted by Eq. 8.10 because of absorption of photons in the aerogel block. According to Eq. 8.9, the number of photoelectrons should be proportional to β^{-2}. The data plotted in Fig. 8.10c nicely confirms this.

Figure 8.8 A large Cerenkov counter system used in the TASSO spectrometer. (H. Burkhardt et al., Nuc. Instr. Meth. 184: 319, 1981.)

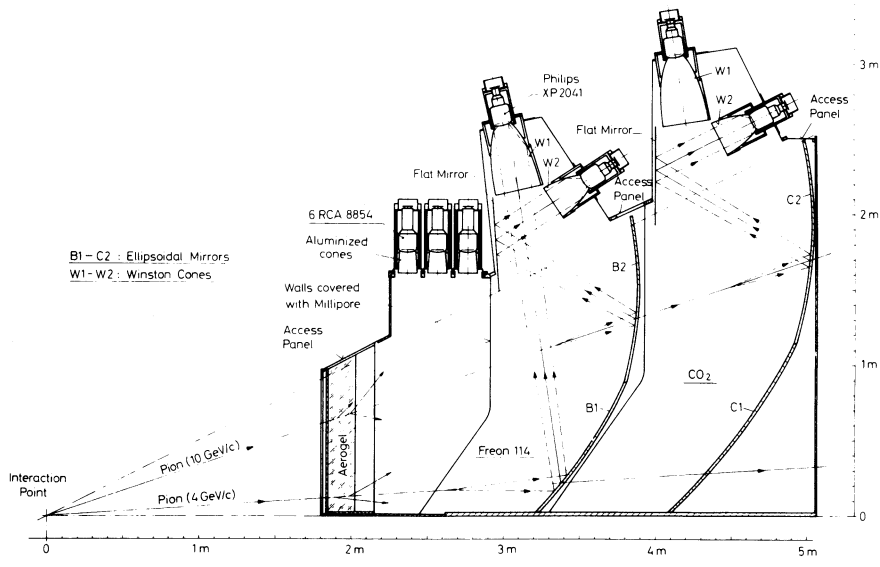

https://doi.org/10.1017/9781009290098.009 Published online by Cambridge University Press

Figure 8.9 Measured Cerenkov counter efficiency as a function of particle momentum. (H. Burkhardt et al., Nuc. Instr. Meth. 184: 319, 1981.)

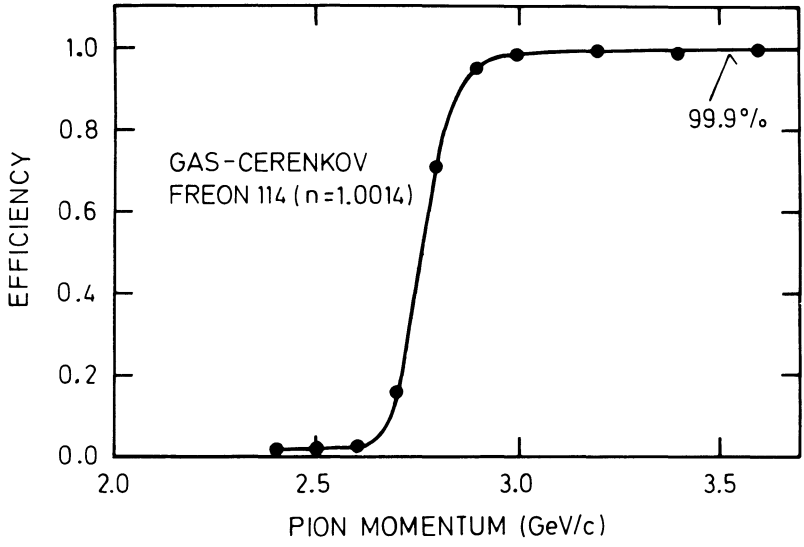

Figure 8.10 (a) Threshold curve for the TASSO aerogel counter, (b) mean number of photoelectrons as a function of the aerogel thickness, and (c) dependence of the mean number of photoelectrons on the quantity β^{-2}. (H. Burkhardt et al., Nuc. Instr. Meth. 184: 319, 1981.)

a

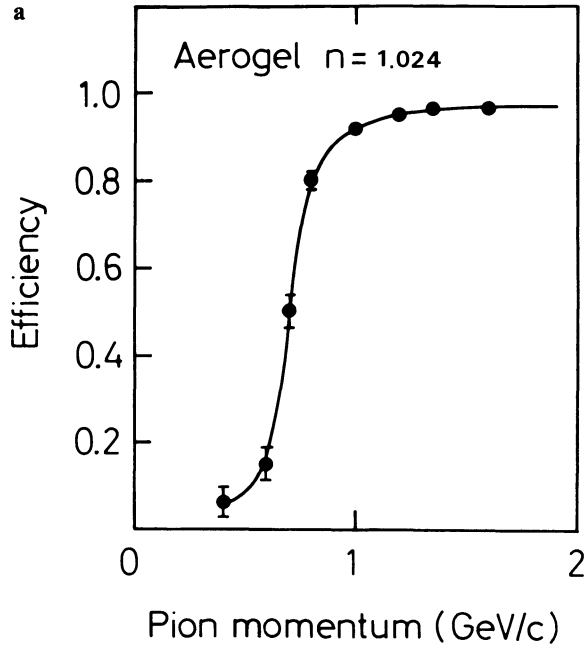

(continued)

https://doi.org/10.1017/9781009290098.009 Published online by Cambridge University Press

Figure 8.10 *Continued.*

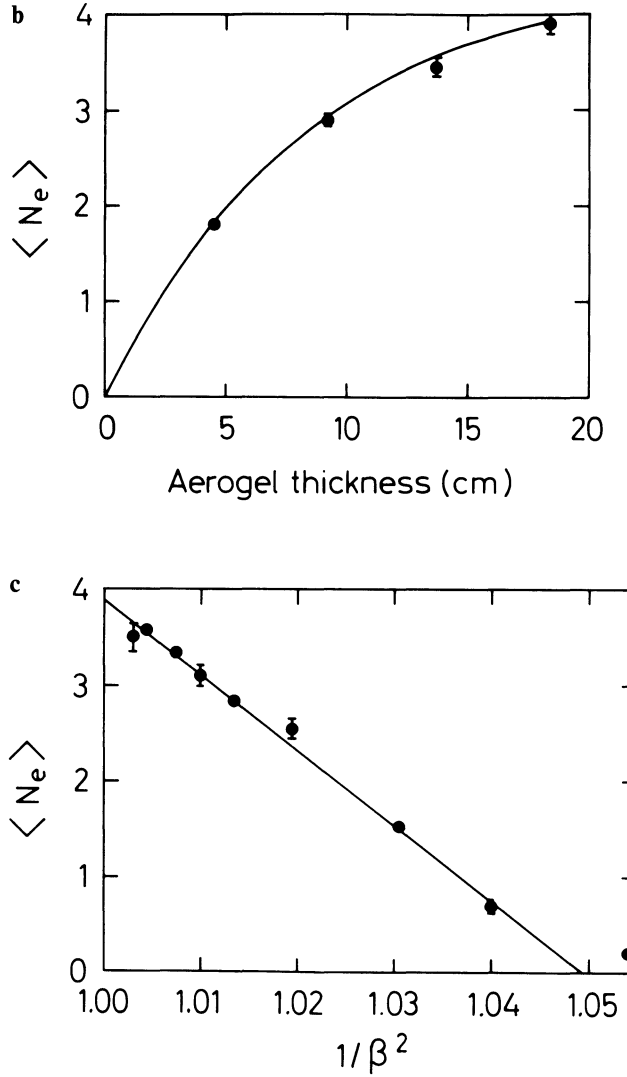

8.5 Differential counters

A differential Cerenkov counter can measure the velocity of a particle by only accepting Cerenkov light in a small annulus around some angle θ. Using such a counter, it is possible to provide a signal for the presence of a given mass particle. The primary design consideration involves the rejection of particles outside the desired mass range. Benot, Litt, and Meunier [9] have given a detailed comparison of the design

https://doi.org/10.1017/9781009290098.009 Published online by Cambridge University Press

criteria of threshold and differential counters. Differential counters are usually designed so that the velocity resolution is no more than one-half of the velocity separation between the closest mass particles it is desired to identify. This must be done for the highest operating momentum.

A simple differential counter was shown in Fig. 8.4. Cerenkov light in the radiator gas is reflected by a spherical mirror. The cones of light appear to the mirror as a ring source at infinity. The image consists of a ring in the focal plane of the mirror with radius

$$r = f \tan \theta \tag{8.33}$$

where f is the focal length of the mirror. The radius of curvature of a spherical mirror is $2f$.

A diaphragm containing a slit of width Δr placed in front of the PMTs will only accept light from within the angular range $\Delta\theta$ given by

$$\Delta\theta = \cos^2\theta \, \Delta r/f \tag{8.34}$$

which corresponds at a given refractive index n to a velocity resolution of

$$\Delta\beta/\beta = \tan \theta \, \Delta\theta \tag{8.35}$$

This shows that small θ and/or $\Delta\theta$ are required for good velocity resolution. On the other hand, we have seen that the photon yield increases like θ^2, so that the counter design must be carefully optimized.

The minimum obtainable angular resolution is mainly limited by dispersion. The indices of refraction of all materials are a function of the wavelength. Differentiating Eq. 8.1, we find that the dispersion limitation is

$$\Delta\theta_{\text{disp}} = \frac{\Delta n}{n \tan \theta} \tag{8.36}$$

where n is the average index of refraction and Δn is the range of n corresponding to the range of accepted wavelengths. The angular resolution is also affected by beam divergence, optical aberrations, multiple scattering in the radiator, energy loss in the radiator, and diffraction [4]. Gases with small optical dispersion include helium, neon, and SF_6, while gases with small multiple scattering include hydrogen, methane, and helium [9].

Figure 8.11 shows a differential gas counter (DISC) used in a hyperon beam at CERN. This counter uses an adjustable optical system to correct for dispersion and geometric aberrations. The accepted velocity could be changed by varying the pressure in the counter. Figure 8.12 shows the particle yield as a function of the velocity. Note the clear separation of different mass particles. A velocity resolution $\Delta\beta \sim 5 \times 10^{-5}$ was achieved.

The DISC counter is only suitable for use in a well-collimated beam of

https://doi.org/10.1017/9781009290098.009 Published online by Cambridge University Press

particles. However, it would clearly be desirable to use the Cerenkov effect to measure the velocities of secondary particles arising from an interaction. This information could then be combined with an independent measurement of the momenta to identify the particles' masses.

One scheme [10] for constructing such a ring imaging Cerenkov (RICH) counter is shown in Fig. 8.13. The radiating medium is contained between two spheres surrounding the target or intersection point. The Cerenkov light reflects off the mirror and is focused onto a ring at the detector surface. With this geometry the radius of the ring is directly related to the Cerenkov angle through Eq. 8.33. The resolution on the relativistic γ factor is [10]

$$\frac{\Delta\gamma}{\gamma} = \frac{\gamma^2\beta^3 n}{\sqrt{N_0 L}} \frac{2\,\Delta r}{R} \tag{8.37}$$

Figure 8.11 A DISC type differential Cerenkov counter. (M) mirror, (C) correction optics, (D) diaphragm, and (P) photomultiplier tube. (J. Litt and R. Meunier, adapted with permission from the Annual Reviews of Nuclear Science, Vol. 23, © 1973 by Annual Reviews, Inc.)

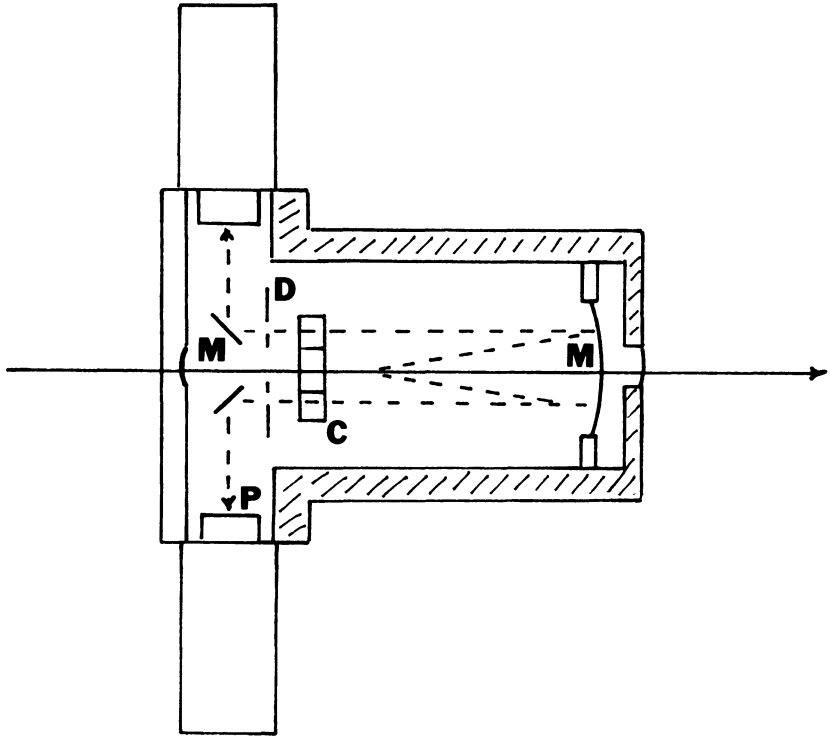

https://doi.org/10.1017/9781009290098.009 Published online by Cambridge University Press

Figure 8.12 A pressure curve for the DISC counter shown in Fig. 8.11. (J. Litt and R. Meunier, adapted with permission from the Annual Reviews of Nuclear Science, Vol. 23, © 1973 by Annual Reviews, Inc.)

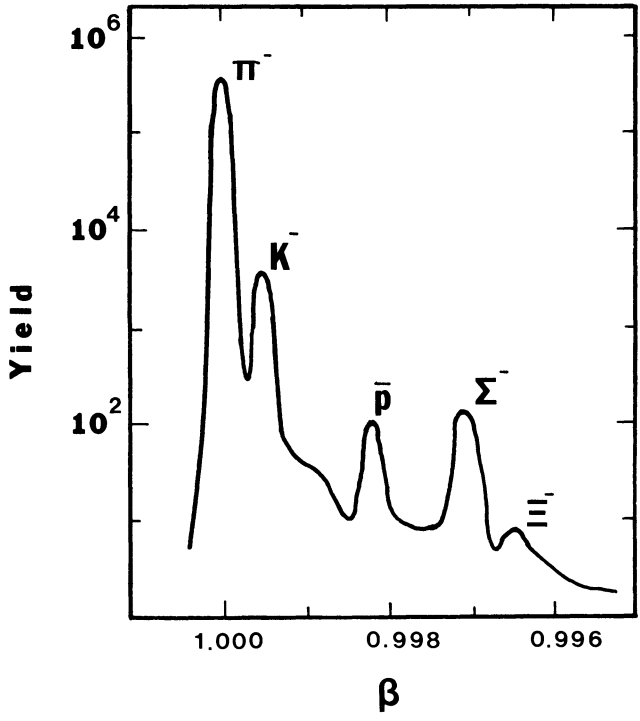

Figure 8.13 Geometrical arrangement for a ring imaging Cerenkov counter. (B) beam, (T) target, (M) spherical mirror, (*R*) radius of M, (P) produced secondary particle, (D) detector plane, and (r) Cerenkov ring on D.

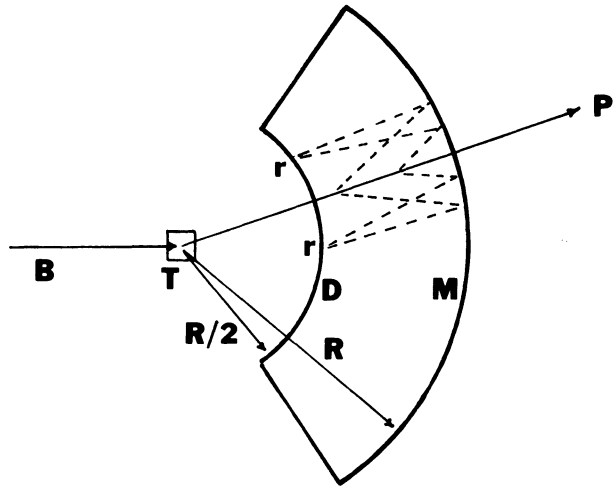

https://doi.org/10.1017/9781009290098.009 Published online by Cambridge University Press

where N_0 and L are given in Eq. 8.10, R is the radius of curvature of the mirror, and Δr is the uncertainty in the ring radius at the detector plane due to all sources. In principle, if external tracking chambers are available, the center of a particle's ring is known, and the detection of only one photon is sufficient to determine the radius of the ring. However, because of complications arising from particle multiplicity and detector inefficiencies, a practical detector design would require several detected photons to determine a ring.

Since the number of photons expected per particle turns out to be very small, most RICH designs have concentrated on collecting photons from the ultraviolet portion of the spectrum. First, according to Eq. 8.4 the photon yield is much larger in the ultraviolet than in the visible. A second reason is that ultraviolet photons can be converted with practically 100% quantum efficiency using the photoelectric effect.

The Cerenkov radiating gas must be transparent in the ultraviolet. This restricts the radiator to a few gases, including the noble gases and nitrogen. The radiator must be separated from the detector by a window made from a material, such as LiF or MgF_2, that is also transparent to the ultraviolet. The detector must have a high efficiency for single photon detection. Proportional chambers, drift chambers, and Geiger needles have all been

Table 8.5. *Ultraviolet photoionization thresholds*

	Ionization threshold	
Gas	(eV)	(nm)
TMAE	5.36	231
TMPD	6.1	203
Perylene	6.95	178
Pyrathrene	7.0	177
Tri-*n*-propylamine	7.2	172
Trimethylamine	7.50	165
Dimethylamine	8.2	151
Methylamine	8.9	139
Benzene	9.24	134
Acetone	9.69	128
Ethanol	10.49	118
Ethane	11.5	108
Methane	12.6	98
Carbon dioxide	13.77	90

Source: A. Breskin et al., Nuc. Instr. Meth. 161: 19, 1979; A. Etkin et al., in Proc. of 1977 ISABELLE Summer Workshop, BNL report 50721, 1977, p. 72.

used. The gas in the detector must have a high efficiency for converting the ultraviolet photons.

Table 8.5 gives the photoionization thresholds for various gases. Only photons whose wavelengths are smaller than the threshold are able to ionize the gas. Three materials with small window thresholds are LiF, MgF_2, and CaF_2. Light is only efficiently transmitted for wavelengths greater than the window limit. Taken together only a narrow range of photon wavelengths can ionize the gas. A small percentage of benzene or other additive with a large photoionization cross section can be used to sensitize wire chambers. Ideally the detector readout should be 2-dimensional. However, some information is still obtained with a 1-dimensional readout, since the projection of the ring creates a double peak spectrum.

8.6 Total absorption counters

In a total absorption Cerenkov counter the incident particle is absorbed in the radiator medium. Two classes of reactions are commonly used with total absorption counters. The first involves incident electrons or photons. These particles initiate an electromagnetic shower through the combined processes of bremsstrahlung and pair production. The Cerenkov radiation emitted by electrons in the shower is detected by the counter. In the second type of reaction the incident particle interacts in the medium and one of the final state particles in the interaction emits the Cerenkov radiation. Examples of such secondary particles include the recoil proton in neutron elastic scatters and electrons produced in neutrino interactions.

Nemethy et al. [11] have constructed a large total absorption water Cerenkov counter for use as a neutrino detector at LAMPF. The counter was required to detect low energy electrons or positrons created in neutrino interactions on free protons or deuterons. A Cerenkov counter was chosen over a scintillation counter for this application in order to avoid background signals from recoil protons in fast neutron interactions.

The counter consisted of 6000 l of water enclosed in a cubic volume with 1.8-m sides. The walls were made of cast epoxy, strengthened by a series of struts. Wavelength shifter was mixed with the water and viewed by 96 PMTs. A fiber-optic light guide was bonded to each tube for calibration purposes. The counter surface not covered by PMTs was covered with a diffuse white reflector. The counter was surrounded by scintillation counters in order to veto cosmic ray events. The counter had a gain of 5.3 photoelectrons/MeV of energy loss. The response was uniform to within 5%. The energy resolution for electrons was $\sigma/E = 12\%$.

Arrays of lead-glass blocks are widely used detectors for photons and electrons. Lead-glass contains about 50% lead by weight. The addition of this high Z element to the glass greatly reduces the radiation length without seriously affecting the transmission of the Cerenkov radiation through the block. Typical values for the density, refractive index, and radiation length of lead-glass are $\rho = 3.9$ g/cm^3, $n = 1.7$, and $L_r = 2.6$ cm. Each block is connected to a PMT. The blocks must be long enough to contain a large fraction of the electromagnetic shower. Arrays of such blocks can cover a large solid angle. The spatial resolution depends on the cross section of the blocks. Fine granularity is usually necessary to resolve the photons originating from π^0 decays. The pulse height of the PMT is proportional to the energy of the incident particle in a properly designed counter. The energy resolution of a lead-glass counter will depend on the amount of shower leakage out of the block and on the photoelectron statistics. The energy resolution varies with energy according to the relation

$$\frac{\sigma(E)}{E} = a + \frac{b}{\sqrt{E}} \tag{8.38}$$

A typical value for b is 10–12%. Intense radiation causes lead-glass to darken.

Two lead-glass arrays were used as photon detectors at the European Hybrid Spectrometer at CERN [12]. One photon detector was designed to simultaneously measure the position and energy of an electromagnetic shower. It consisted of a 2-dimensional array of $5 \times 5 \times 42$ cm^3 lead-glass blocks mounted on a movable platform. The blocks were arranged longitudinally to the beam in order to totally absorb the shower. A diagram of one counter is shown in Fig. 8.14. Light is transmitted through a lead-glass light guide to the PMT. The gain of each counter was monitored using a laser–optical fiber calibration system. Spatial resolution was im-

Figure 8.14 Design of an EHS lead-glass counter. (B. Powell et al., Nuc. Instr. Meth. 198: 217, 1982.)

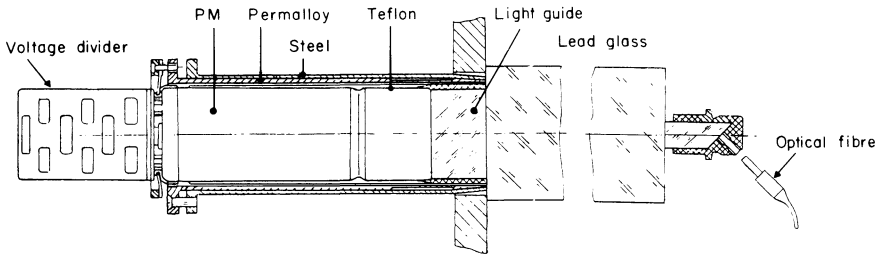

https://doi.org/10.1017/9781009290098.009 Published online by Cambridge University Press

proved by accurately measuring the small amplitude tails on either side of the main shower deposition. The measured spatial resolution was 3.7 mm(FWHM), while the energy resolution was $\Delta E/E = 0.15/\sqrt{E} + 0.02$ (FWHM).

References

[1] J. Jelley, *Cerenkov Radiation and its Applications,* London: Pergamon, 1958.
[2] V. Zrelov, *Cherenkov Radiation in High Energy Physics,* Israel Program for Scientific Translations, Federal Scientific and Technical Information, Springfield, VA, 1970.
[3] V. Zrelov, M. Klimanova, V. Lupiltsev, and J. Ruzicka, Calculations of threshold characteristics of Vavilov-Cherenkov radiation emitted by ultrarelativistic particles in a gaseous Cherenkov counter, Nuc. Instr. Meth. 215: 141–6, 1983.
[4] J. Litt and R. Meunier, Cerenkov counter technique in high energy physics, Ann. Rev. Nuc. Sci. 23: 1–43, 1973.
[5] W. Galbraith, Cerenkov counters, in High Energy and Nuclear Physics Data Handbook, Sec 6, National Institute for Research in Nuclear Science, Rutherford Laboratory, 1963.
[6] The applicability of threshold counters to high energy colliders such as LEP is considered in P. Lecomte, G. Poelz, R. Riethmuller, O. Romer, and P. Schmuser, Threshold Cerenkov counters, Physica Scripta 23: 377–83, 1981.
[7] H. Burkhardt, P. Koehler, R. Riethmuller, B. Wiik, R. Fohrmann, J. Franzke, H. Krasemann, R. Maschuw, G. Poelz, J. Reichardt, J. Ringel, O. Romer, R. Rusch, P. Schmuser, R. van Staa, J. Freeman, P. Lecomte, T. Meyer, S. Wu, and G. Zobernig, The TASSO gas and aerosol Cherenkov counters, Nuc. Instr. Meth. 184: 319–31, 1981.
[8] G. Poelz and R. Riethmuller, Preparation of silica aerosol for Cherenkov counters, Nuc. Instr. Meth. 195: 491–503, 1982.
[9] M. Benot, J. Litt, and R. Meunier, Cherenkov counters for particle identification at high energy, Nuc. Instr. Meth. 105: 431–44, 1972.
[10] J. Seguinot and T. Ypsilantis, Photoionization and Cherenkov ring imaging, Nuc. Instr. Meth. 142: 377–91, 1977; T. Ypsilantis, Cerenkov ring imaging, Physica Scripta 23: 371–6, 1981.
[11] P. Nemethy, S. Willis, J. Duclos, and H. Kaspar, A water Cerenkov neutrino detector, Nuc. Instr. Meth. 173: 251–7, 1980.
[12] B. Powell, R. Heller, N. Ibold, K. Schubert, J. Stiewe, M. Vysocansky, M. Mazzucato, P. Rossi, L. Ventura, G. Zumerle, M. Boratav, J. Duboc, J. Passeneau, M. Touboul, P. Bagnaia, C. Dionisi, D. Zanello, L. Zanello, V. Bujanov, Y. Fisjak, A. Kholodenko, E. Kistenev, B. Poljakov, E. Castelli, P. Checchia, and C. Troncon, The EHS lead-glass calorimeters and their laser based monitoring system, Nuc. Instr. Meth. 198: 217–31, 1982.

Exercises

1. Find the Cerenkov angles for 2-GeV/c pions in water, lucite, and NaI.

2. Find the total Cerenkov energy emitted in visible wavelengths by a 1-GeV/c proton crossing 1 m of water.

3. Design a Cerenkov counter that gives on the average 10 collected photoelectrons for 5-GeV/c kaons.

4. Plot the convoluted frequency response of the RCA 8575 tube for Cerenkov radiation.

5. A kaon beam passes through a 2-m-long Cerenkov counter that contains CO_2 at 2 atm and has a quality factor $N_0 = 400\ \text{cm}^{-1}$. At what momentum should the efficiency of the counter reach 50%?

6. Consider a 1-GeV/c proton passing through water. Calculate numerically the number of visible photons emitted by δ rays. Use an approximation for dE/dx over the relevant energy range.

7. An atmospheric pressure, helium differential Cerenkov counter has a spherical mirror of radius 2 m and a 1-mm acceptance slit. What is the expected velocity resolution?

8. Design a total internal reflection counter that accepts *all* particles whose velocity exceeds a minimum threshold. How can you maximize the quality factor N_0? How should the radiator be coupled to the PMT?